PROCEEDINGS, 46th Workshop on Geothermal Reservoir Engineering
Stanford University, Stanford, California, February 15-17, 2021
SGP-TR-

# Inferring fracture aperture distribution at the EGS Collab Experiment 1 testbed through a deep learning accelerated Bayesian approach

Hui Wu, Jize Zhang, Pengcheng Fu, Joseph P. Morris, the EGS Collab Team

Atmospheric, Earth, and Energy Division, Lawrence Livermore National Laboratory, Livermore, CA 94550

E-mail address: wu40@llnl.gov

**Keywords:** EGS, tracer test, aperture distribution, MCMC, uncertainty.

## ABSTRACT

Fracture aperture is an essential characteristic for fluid flow, mass transport and heat transfer processes in fractured reservoirs, and the characterization of fracture aperture is a critical task for energy recovery from subsurface fractured reservoirs. As direct measurement is usually sparse or even unavailable, the aperture distribution in subsurface fractures can only be inferred from geophysical observations and *in situ* flow (or pressure) and tracer tests. In the present study, we explore the feasibility of inferring aperture distribution in a hydraulic fracture from tracer tests through Markov Chain Monte Carlo (MCMC). The following two strategies were used to alleviate the notorious computational burden of MCMC. First, we performed principal component analysis (PCA) on spatially-correlated aperture distributions to map the original high-dimensional aperture distribution to a latent space with relatively low dimensionality. Second, a surrogate model for tracer transport in the hydraulic fracture was developed using convolutional neural network (CNN) and then applied to MCMC to improve inference efficiency. Field data from the ongoing EGS Collab project was used to demonstrate the efficacy of MCMC in aperture inference. Tracer breakthrough curves from field tracer tests were appropriately reproduced, and the inferred aperture distribution in the hydraulic fracture varied between 0.1 to 0.24 mm with an uncertainty of approximately 0.04 to 0.1 mm.

## 1. INTRODUCTION

Fracture network plays a crucial role in many subsurface reservoir applications such as oil, gas and thermal recovery, $CO_2$ storage and industrial waste disposal (Tsang et al., 2015; Fu et al., 2017; Gierzynski and Pollyea, 2017; Wu et al., 2021). For many subsurface reservoirs such as enhanced geothermal system (EGS), fracture network provides principal pathways for fluid since the permeability of intact rock matrix is very low, and the relevant physical processes such as fluid flow, mass transport and heat transfer largely depend on aperture distributions in the fracture network. The characterization of fracture aperture distribution is therefore a critical step for production optimization, uncertainty quantification and long-term risk management of subsurface reservoirs. As direct aperture measurement is often very sparse or unavailable, fracture aperture in subsurface reservoirs is commonly quantified from the inference of single well or cross well pressure (flow) and tracer tests (Neuman, 2005), either in a deterministic manner (Radilla et al., 2012; Hawkins et al., 2018, 2020) or a stochastic manner (Cacas et al., 1990; Vogt et al., 2012a, 2012b; Chen et al., 2013; Wu et al., 2021).

Bayesian inference such as Markov Chain Monte Carlo (MCMC) has been widely used for subsurface characterization, including permeability inference (Efendiev et al., 2005; Fu and Gómez-Hernández, 2009; Cui et al., 2011; Laloy et al, 2018; Zhang et al., 2020a), fracture network characterization (Somogyvári et al., 2017) and aperture estimation (Shakas et al., 2018). In the Bayesian inference framework, the unknown parameters such as permeability/aperture are treated as random variables, and their posterior distributions can be inferred from observations and measurements according to the Bayes' theorem. MCMC approximates the posterior distribution of the unknown parameters by constructing a Markov chain with the posterior distribution as its target distribution. With the posterior distribution, the spatial distribution of permeability/aperture can be inferred and the associated uncertainties can be quantified. One of the major challenges in MCMC is the computational burden resulting from numerous forward model evaluations. Many methods have been proposed to improve the efficiency of MCMC and reduce the required computational cost. These methods can be categorized into two groups. The first group reduces the time and cost of a single model evaluation by replacing the forward model with a surrogate model (Christen and Fox, 2005; Efendiev et al., 2005; Marzouk and Najm, 2009; Laloy et al., 2013; Zhang et al., 2018; Zhang et al., 2020b). The second group shortens the length of the Markov chain by adopting more efficient proposal algorithms, such as adaptive Metropolis, delayed rejection, differential evolution (Haario et al., 2001; ter Braak and Vrugt, 2008; Lu et al., 2019; Zhang and Taflanidis, 2019; Wu et al., 2020), to name a few. Among these methods, DREAM$_{(ZS)}$ has proven an effective method, which combines differential evolution and adaptive Metropolis and uses a subspace sampling strategy to accelerate the convergence of the Markov chain to the target distribution (Laloy and Vrugt, 2012; Vrugt, 2016).

The main goal of the present study is to infer the aperture distribution of a hydraulically stimulated fracture at the EGS Collab Experiment 1 testbed. The work described in this paper is an extension of our previous work on stochastic tracer modeling (Wu et al., 2021). In this paper, we use a MCMC framework to infer the heterogeneous aperture distribution in the hydraulic fracture from a conservative tracer test. We adopt the DREAM$_{(ZS)}$ method and use the following two strategies to further improve the inference efficiency of DREAM$_{(ZS)}$. First, we use the principal component analysis (PCA) to reduce the original high-dimensional aperture distribution to a low dimensional latent parameter space. Second, we use convolutional neural network (CNN) to construct a fast and accurate surrogate model to replace the forward model for tracer transport in the hydraulic fracture. In what follows, Section 2 briefly introduces the EGS Collab Experiment 1 testbed and the previous analysis of fracture characteristics by Wu et al. (2021). Section 3 describes the methodologies in the present study, including the main components of DREAM$_{(ZS)}$, the generation of spatially-autocorrelated aperture distributions, dimensionality

reduction of the aperture distribution through PCA, and the development of a surrogate model through CNN. In Section 4, we present the posterior distributions of the latent parameters and the corresponding aperture distribution as well as the associated uncertainty.

## 2. EGS COLLAB EXPERIMENT 1 AND PREVIOUS ANALYSIS OF FRACTURE CHARACTERISTICS

The EGS Collab project is an ongoing *in situ* experiment designed to investigate the stimulation of fracture networks in rocks and circulation of fluids in these fracture networks at an intermediate scale (Kneafsey et al., 2019; White et al., 2019). The Experiment 1 of the project was performed in a predominately phyllite rock, approximately 1478 m below ground surface, on the western side of the West Access Drift at the 4850 Level within the Sanford Underground Research Facility (SURF) in South Dakota, USA. The geological conditions of the Experiment 1 testbed, wellbore configuration and geophysical measurements have been sufficiently described in previous studies (Kneafsey et al., 2020; Schoenball et al., 2020; Wu et al., 2021) and therefore not repeated here.

A series of hydraulic stimulations, tracer tests and water circulation tests were conducted between May 2018 and February 2020 (Kneafsey et al., 2020; Neupane et al., 2020; Wu et al., 2021). According to various geological/geophysical observations and measurements during these tests, such as core logs, wellbore images, microseismic events, distributed temperature sensing (DTS) and sewer camera survey, Wu et al. (2021) developed a fracture network model involving a hydraulic fracture (HF) and a predominant natural fracture (NF) (Fig. 1(a)) for the Experiment 1 testbed. Fig. 1(a) also annotates the injection well (E1-I), production well (E1-P) and monitoring wells (E1-OT, E1-PST, E1-PSB, E1-PDT and E1-PDB) intersecting the fracture network. Note that E1-P intersected HF at E1-PB and NF at E1-PI. Multiple tracer tests were conducted as summarized in Neupane et al. (2020). In the present study, we focus on a conservative tracer test conducted on October 31, 2018. In this tracer test, 0.64 g C-Dots were first mixed with water and then injected into the fracture network through E1-I with an injection rate of 400 ml/min and an injection concentration of $C_0$ = 305 ppm. Fig. 1(b) shows the measured tracer breakthrough curves at E1-OT, E1-PB and E1-PI, as well as outflow rates at different wells during the tracer test. To interpret the tracer data, Wu et al. (2021) assumed elliptical shapes for HF and NF, and used a leakage interface to represent their interactions. The aperture distributions in HF and NF were analyzed separately. The HF was parameterized by the following parameters: $A_1$ and $A_2$ for the semi-axis lengths of HF, $w$ for fracture aperture, $\alpha_L$ for longitudinal dispersivity, $\theta$ and $L$ for the location and length of a pressure sink on the periphery of HF accounting for fluid/tracer leakage to other natural fractures that are not explicitly described in the model, $P_L$, $L_L$ and $q_L$ for the location, length and leakage rate of the leakage interface (Fig. 1(c)). With the tracer measurements in Fig. 1(b), Wu et al. (2021) inverted for the values of the above parameters using stochastic tracer modeling. They first assumed a uniform aperture in the hydraulic fracture, and the optimal realization that best matched the tracer measurements indicated the following parameter values: $A_1$ = 15.8 m, $A_2$ = 12.3 m, $w$ = 0.167 mm, $\alpha_L$ = 0.136 m, $\theta$ = 240°, $L$ = 14.5 m, $P_L$ = 6.2 m, $L_L$ = 5.6 m and $q_L$ = 186 mL/min. They then assumed a heterogeneous aperture distribution. Multiple satisfactory realizations were obtained, but the aperture distributions among these realizations showed different patterns.

The focus of the present study is using MCMC to infer the heterogeneous aperture distribution in the hydraulic fracture from the tracer test on October 31, 2018. We only model the tracer transport in the hydraulic fracture, and therefore the tracer breakthrough curves at E1-OT and E1-PB in Fig. 1(b) are used as measurements. The parameterization of the hydraulic fracture is the same as that in Wu et al. (2021), as shown in Fig. 1(c). Spatially-autocorrelated aperture fields following log-normal distributions are assumed in the hydraulic fracture, and other parameters are fixed at the values inferred from the above-mentioned optimal realization under the uniform aperture scenario.

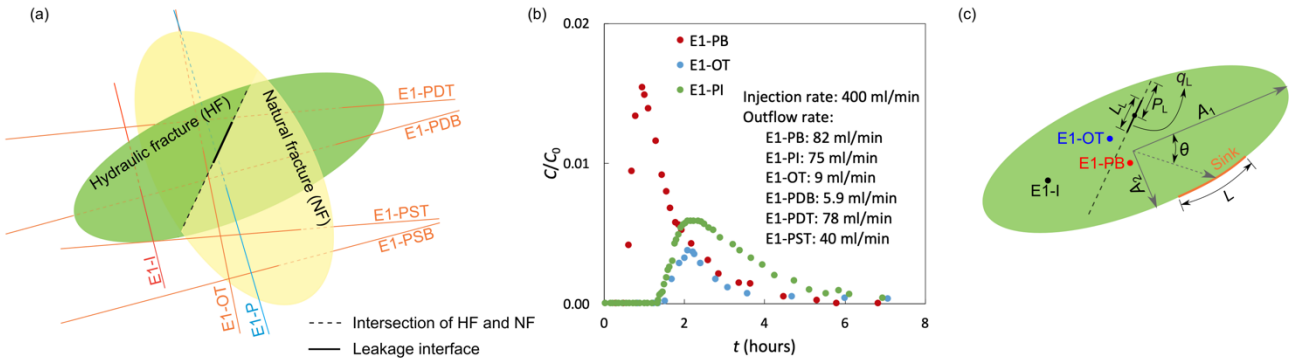


**Figure 1: (a) Fracture network model from Wu et al. (2020). E1-I is the injection well, E1-P is the production well, and E1-OT, E1-OB, E1-PDT, E1-PDB, E1-PST and E1-PSB are six monitoring wells. (b) Tracer breakthrough curves from a conservative tracer test conducted on October 31, 2018. Injection rate and outflow rates at different wells are annotated. (c) Parameterization of the hydraulic fracture.**

## 3. METHODOLOGIES

### 3.1 Inference framework of MCMC

MCMC combines prior information with information from measurements and from the theoretical physical relationship between parameters and model responses, and infers the posterior distribution of model parameters according to the Bayes' theorem. In the framework of MCMC, the physical relationship can be represented by the following form,

$$\mathbf{e} = F(\mathbf{z}) - \mathbf{d} \qquad (1)$$

where **e** is measurement errors, **z** is the unknown model parameters, $F$ represents the forward model, and **d** is the measurements. In the current study, **z** is the parameters for aperture distribution in the hydraulic fracture, $F$ is the tracer transport model, and **d** is the field tracer breakthrough curves at E1-OT and E1-PB in Fig. 1(b). According to the Bayes' theorem, the posterior distribution of model parameters $p(\mathbf{z}|\mathbf{d})$ can be written as,

$$p(\mathbf{z}|\mathbf{d}) = \frac{p(\mathbf{z})p(\mathbf{d}|\mathbf{z})}{\int p(\mathbf{z})p(\mathbf{d}|\mathbf{z})d\mathbf{z}} \propto p(\mathbf{z})L(\mathbf{d}|\mathbf{z}) \qquad (2)$$

where $p(\mathbf{z})$ is the prior distribution of model parameters, representing our knowledge of the model parameters before any measurement is obtained. $L(\mathbf{d}|\mathbf{z})$ is the likelihood function, which evaluates the goodness-of-fit between model responses $F(\mathbf{z})$ and measurements **d**. If we assume the measurement error **e** to be independent, identically distributed Gaussian random variables, $L(\mathbf{d}|\mathbf{z})$ can be expressed as,

$$L(\mathbf{d}|\mathbf{z}) = \Pi_{i=1}^{N} \frac{1}{\sqrt{2\pi}\sigma_i} \exp\left(-\frac{1}{2\sigma_i^2}[d_i - F_i(\boldsymbol{z})]^2\right) \qquad (3)$$

where $N$ is the number of measurements, $\sigma_i$ is the $i$th element of the standard deviation of **e**, $d_i$ and $F_i(\boldsymbol{z})$ are the $i$th elements of **d** and $F(\mathbf{z})$ respectively. In the current study, we set $\sigma_i = 0.01$.

A traditional method to construct a Markov chain with a stationary distribution of $p(\mathbf{z}|\mathbf{d})$ is the Metropolis-Hastings algorithm (Metropolis et al., 1953; Hastings, 1970), which includes the following steps: 1) At the initial iteration ($i$ = 0), draw an initial parameter sample $\mathbf{z}_0$ from the prior distribution $p(\mathbf{z})$. 2) At iteration $i$ ($i$ > 0), propose a new parameter sample $\mathbf{z}'$ from a proposal distribution $q(\mathbf{z}'|\mathbf{z}_{i-1})$. 3) Accept the new parameter sample $\mathbf{z}'$ with the probability: $\alpha(\mathbf{z}, \mathbf{z}') = \min[1, \frac{p(\mathbf{z}')L(\mathbf{d}|\mathbf{z}')q(\mathbf{z}_{i-1}|\mathbf{z}')}{p(\mathbf{z}_{i-1})L(\mathbf{d}|\mathbf{z}_{i-1})q(\mathbf{z}'|\mathbf{z}_{i-1})}]$. 4) If $\mathbf{z}'$ is accepted, set $\mathbf{z}_i = \mathbf{z}'$. Otherwise, set $\mathbf{z}_i = \mathbf{z}_{i-1}$. 5) Set $i = i + 1$ and repeat steps (2) ~ (4) until the maximum iteration number is reached. Detailed balance and ergodicity of the Metropolis-Hastings algorithm have been widely studied, and the convergence of the Markov chain to $p(\mathbf{z}|\mathbf{d})$ after burn-in period is guaranteed (Zhang et al., 2019).

The sampling efficiency of MCMC greatly depends on the proposal distribution $q(\mathbf{z}'|\mathbf{z}_{i-1})$. In the current study, we adopt the DREAM$_{(ZS)}$ algorithm to construct Markov chains. DREAM$_{(ZS)}$ combines differential evolution, subspace sampling, and snooker proposal distributions to general new parameter samples from Markov chain history, and has proved an efficient MCMC algorithm (Laloy and Vrugt, 2012; Vrugt, 2016). The details of DREAM$_{(ZS)}$ are described in Vrugt (2016) and therefore not repeated here.

### 3.2 Dimensionality reduction of spatially-autocorrelated aperture fields

Fracture aperture has been widely studied in the literature (Moreno et al., 1988; Pyrak-Nolte and Morris, 2000; Tsang and Tsang, 1989). According to the measurements of core samples and observations of well logs, fracture aperture is generally spatially-autocorrelated and typically follows a gamma distribution or a log-normal distribution (Bianchi and Snow, 1968; Gale, 1987). In the current study, we use sequential gaussian simulation to generate spatially-autocorrelated aperture fields following a log-normal distribution from spherical variogram with a mean of 0.167 mm, a standard deviation of 0.167 mm and a correlation length of 8 m. Note that we do not consider the anisotropy of the aperture field, indicating that the correlation lengths along different directions are identical. The aperture field is first generated on a 161 × 161 regular mesh, and then applied to the hydraulic fracture model in Fig. 1(c). Fig. 2(a) shows an example of the spatially-autocorrelated aperture field. The extent of the hydraulic fracture is also plotted. Note that only the aperture field within the hydraulic fracture extent is effective in subsequent tracer transport modeling.

The hydraulic fracture in Fig 2(a) consists of 11054 elements. Dimensionality reduction is necessary for the following two reasons. First, such a high-dimensional inference problem is challenging and might be intractable. Second, treating aperture values as independent parameters does not honor the spatial autocorrelation characteristics of aperture distribution. Different dimensionality reduction approaches have been used to mapping high-dimensional, spatially-autocorrelated fields to low-dimensional latent parameter spaces, including Karhunen-Loève expansion (Zhang and Lu, 2004; Efendiev et al., 2005; Laloy et al., 2013), principal component analysis (PCA) (Hawkins et al., 2020), and deep learning based approaches such as variational autoencoder (VAE) (Laloy et al., 2017; Canchumuni et al., 2021) and adversarial generative network (GAN) (Laloy et al., 2018; Mo et al., 2020). Because the aperture distribution in the current study follows a multi-Gaussian distribution, we use PCA to map the original aperture field to a latent parameter space, represented by a vector $\boldsymbol{\xi}_l$ with a dimensionality of $l$. The details of PCA are described in Liu and Durlofsky (2020). The main procedures include:

1) Generate an ensemble of $N_r$ spatially-autocorrelated fields $\mathbf{Z} = \{\mathbf{z}_1, \mathbf{z}_2, \ldots, \mathbf{z}_{N_r}\}$using sequential gaussian simulation.

2) Assemble the fields into a centered matrix:

$$\mathbf{Y} = \frac{1}{\sqrt{N_r - 1}}\left[\mathbf{z}_1 - \bar{\mathbf{z}} \;\; \mathbf{z}_2 - \bar{\mathbf{z}} \;\ldots\; \mathbf{z}_{N_r} - \bar{\mathbf{z}}\right] \qquad (4)$$

where $\mathbf{Y} \in \mathbb{R}^{N_c \times N_r}$, $N_c$ is dimensionality of the spatially-autocorrelated field, $\bar{\mathbf{z}}$ is the mean of the $N_r$ fields.

3) Perform singular value decomposition on **Y**: $\mathbf{Y} = \mathbf{U}\boldsymbol{\Sigma}\mathbf{V}^T$, where $\mathbf{U} \in \mathbb{R}^{N_c \times N_r}$ and $\mathbf{V} \in \mathbb{R}^{N_r \times N_r}$ are the left and right singular matrices, $\boldsymbol{\Sigma} \in \mathbb{R}^{N_r \times N_r}$ is a diagonal matrix whose diagonal elements are singular values.

4) Use the first $l$ columns in **U**, $\mathbf{U}_l \in \mathbb{R}^{N_c \times l}$, and a diagonal matrix $\boldsymbol{\Sigma}_l \in \mathbb{R}^{l \times l}$ which contains the first $l$ singular values in $\boldsymbol{\Sigma}$ as the basis to reconstruct original fields and generate new fields.

5) To reconstruct an original aperture field $\mathbf{z}_i$, first calculate the latent parameter vector $\boldsymbol{\xi}_l^i$:

$$\boldsymbol{\xi}_l^i = \boldsymbol{\Sigma}_l^{-1}\mathbf{U}_l^T(\mathbf{z}_i - \bar{\mathbf{z}}) \qquad (5)$$

The aperture field $\mathbf{z}_i$ can then be reconstructed as:

$$\hat{\mathbf{z}}_i = \bar{\mathbf{z}} + \mathbf{U}_l\boldsymbol{\Sigma}_l\boldsymbol{\xi}_l^i \qquad (6)$$

where $\hat{\mathbf{z}}_i$ is the reconstructed aperture field.

5) New aperture field can be generated from the following form:

$$\mathbf{z}_{\mathrm{PCA}} = \bar{\mathbf{z}} + \mathbf{U}_l\boldsymbol{\Sigma}_l\boldsymbol{\xi}_l \qquad (7)$$

where $\boldsymbol{\xi}_l$ is a $l$-dimensional latent parameter vector with each element independently sampled from standard normal distribution.

The capability of reconstructing an aperture field from equation (6) depends on $l$. If $l$ equals $N_r$, the original aperture field can be fully reconstructed. With the decrease in $l$, the difference between the original and reconstructed aperture fields gradually increases. In the current study, we generated 5000 spatially-autocorrelated fields for PCA, and we select the first 100 singular vectors and singular values for aperture field reconstruction and generation, i.e., $l = 100$. Approximately 83% of the total variance or "energy" in the original aperture fields can be preserved (Fig. 2(a)). Fig. 2(c) further shows a new aperture field from equation (7) using a randomly generated 100-dimensional latent parameter.

Correspondingly, the goal of MCMC is to approximate the posterior distribution of the 100-dimensional latent parameter $\boldsymbol{\xi}_l$ according to the tracer breakthrough curves in Fig. 1(b). In each iteration of MCMC, we propose a new latent parameter $\boldsymbol{\xi}'$ and then generate $\mathbf{z}'$ from $\boldsymbol{\xi}'$ through equation (7). The prior distribution of $\boldsymbol{\xi}'$ is the standard normal distribution. Once the posterior distribution of $\boldsymbol{\xi}_l$ is obtained, we can estimate the mean aperture field and its uncertainty by sampling $\boldsymbol{\xi}_l$ from the posterior distribution to generate posterior aperture fields through equation (7).

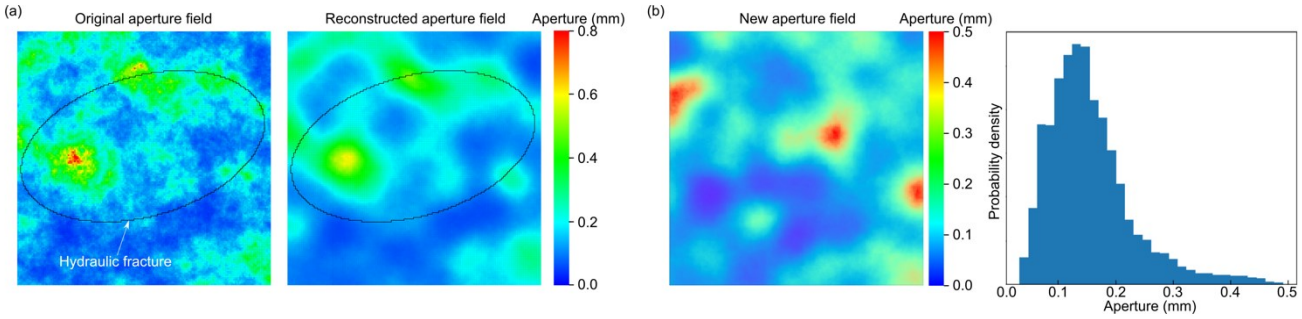


**Figure 2: Dimensionality reduction of aperture fields through PCA. (a) Reconstruction of a spatially-autocorrelated aperture field through the first 100 singular vectors and values from PCA. The extent of the hydraulic fracture is annotated. (b) A new aperture field generated from a 100-dimensional latent parameter and the corresponding histogram.**

### 3.3 Surrogate model for tracer transport in the hydraulic fracture

In each iteration of MCMC, we need to calculate the likelihood $L(\mathbf{d}|\mathbf{z}')$ of the proposed aperture field $\mathbf{z}'$, which requires running the tracer transport model with $\mathbf{z}'$. Wu et al. (2021) described the details of the tracer transport model. The permeability of the hydraulic fracture was calculated from the aperture distribution according to the cubic law. The injection rate and outflow rate in Fig. 1(b) were first used as boundary conditions to solve for a steady state flow field in the hydraulic fracture, and then the tracer injection concentration and duration were used to solve for tracer transport process and obtain the simulated tracer breakthrough curves at E1-PB and E1-OT. According to Wu et al. (2021), the time cost of the tracer transport model on a single core of Xeon E5-2695 v4 varies between less than a minute and several hours, depending on the underlying flow field. To generate a valid Markov chain, the tracer transport model might be called thousands or even tens of thousands of times, leading to an extremely high computational cost.

One approach to addressing the high computational burden is developing a surrogate model to replace the tracer transport model for the calculation of likelihood. Surrogate model has been widely used in many subsurface applications such as contaminant transport in hydrological systems (Zhang et al., 2020), groundwater flow (Laloy et al., 2013), geological carbon sequestration (Mo et al., 2019; Zhong et al., 2019), and reservoir characterization and exploitation (Tang et al., 2020). There are three broad families of surrogate models, including data-driven surrogate models that use function approximation techniques to approximate model responses, projection-based surrogate models that project governing equations onto a reduced dimension subspace characterized by a basis of orthonormal vectors, and low-fidelity surrogate models with simplified physics or reduced numerical resolution. Razavi et al. (2012) and Asher et al. (2015) provided comprehensive reviews of surrogate models. In the current study, we use a deep learning approach to developing a data-driven surrogate model for the tracer transport model in the hydraulic fracture.

We use the Wide ResNet architecture (Zagoruyko and Komodakis, 2017) for its strong performance on benchmark computer vision datasets. Fig. 3 shows the detailed structure of the Wide ResNet. It largely follows the original structure in Zagoruyko and Komodakis, 2017, but with a minor modification to use the adaptive pooling in the final layers for its compatibility with input images of arbitrary resolutions. The input of the Wide Resnet is a 64 × 64 field, which is downscaled from the original 161 × 161 aperture field using bilinear interpolation. Note that the aperture values of cells outside the fracture are set to 0. The output of the Wide Resnet is a scalar which is the sum of the square error between the simulated and measured tracer data. The depth of the Wide Resnet is 16 and the width factor is 2. A dropout rate of 0.3 is used in the present study.

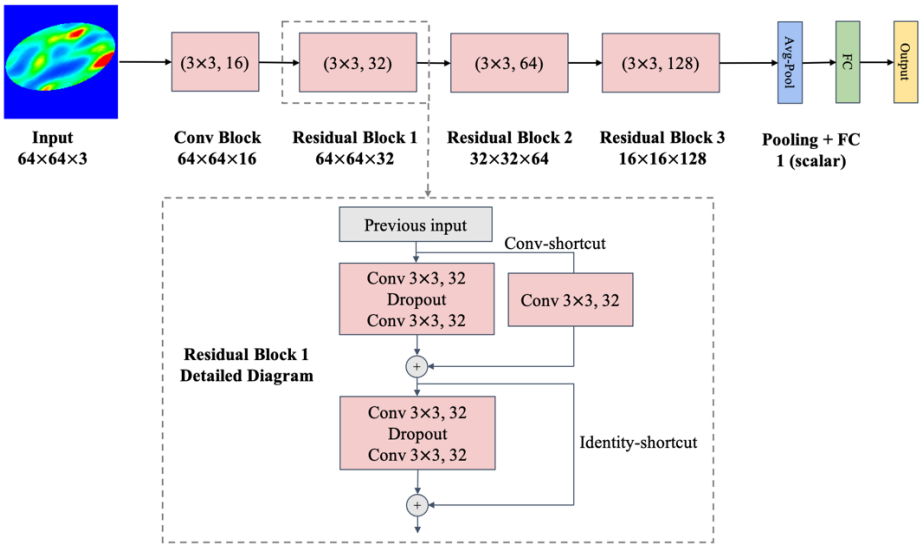


**Figure 3: A Wide ResNet architecture with a depth of 16 and a width of 2. The notation (*k*×*k*, *n*) in the convolutional (Conv) block and residual blocks denotes a filter of size *k* and *n* channels. The dimensionality of outputs from each block is also annotated. The detailed structure of the residual block is shown in the dash line box. Note that batch normalization and ReLU precede the convolution layers and fully connected layer but omitted in the figure for clarity.**

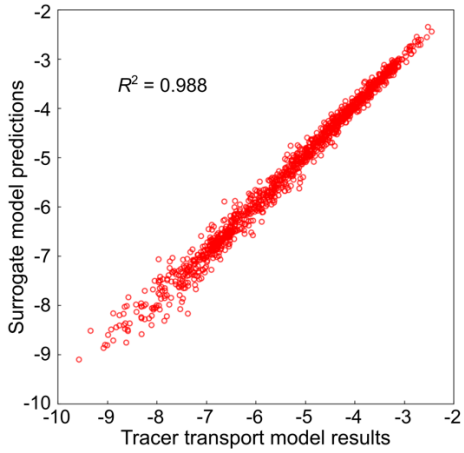


**Figure 4: Comparison of the square error (natural logarithm) of tracer breakthrough curves at E1-PB and E1-OT between tracer transport model results and surrogate model predictions.**

To train the Wide ResNet, we generated 48000 aperture fields through equation (7) as the training inputs. For each of the aperture fields, we first run the tracer transport model to simulate tracer breakthrough curves at E1-PB and E1-OT, and then calculated the sum of the square error $E$ (a scalar) between the simulation results and the measurements using the following equation,

$$E_i = \sum_{j=1}^{N_d} (C_j^s - C_j^m)^2 \qquad (8)$$

Where $C_j^s$ and $C_j^m$ are simulated and measured relative tracer concentrations. $N_d$ is the number of tracer concentration measurements, including both the tracer measurements at E1-PB and E1-OT in Fig. 1(b).

The calculated square errors were provided to the Wide ResNet as training outputs. We randomly divided the available data into two splits of 90% and 10% for training and validation, respectively. Hyperparameters were determined through the HpBandster toolbox, an efficient tool for hyperparameter optimization (Falkner et al., 2018). The learning rate was 0.001, the minibatch size was 64 and the weight decay factor was 0.0005. We used 300 epochs with early stopping mechanism to terminate training when the validation performance did not improve after 100 epochs. After training, we generated 1250 extra pairs of aperture fields and square errors to test the performance of the surrogate model. Fig. 4 compares the surrogate model predictions and the tracer transport model results for the 1250 aperture fields.

## 4. RESULTS AND DISCUSSIONS

### 4.1 Markov chain evolution

DREAM$_{(ZS)}$ requires running multiple parallel chains to enable differential evolution which proposes new parameter samples from different chains. In the current study, we run 10 parallel chains simultaneously to infer the posterior distributions of the 100 latent parameters. After performing DREAM$_{(ZS)}$, each chain contains 8000 parameter samples. Fig. 5 shows the trace plots of the first eight latent parameters in three chains. We use the $\hat{R}$ statistics, which compares the within-chain and between-chain variances (Gelman and Rubin, 1992) to monitor the convergence of the Markov chains. The rule of thumb is that convergence is attained if $\hat{R}$ statistics is smaller than 1.2 for all the parameters. According to this rule, the convergence was attained after 6560 iterations (Fig. 5). In the following analysis, we use the last 500 parameter samples in each of the 10 chains to analyze the posterior distributions of the latent parameters as well as the aperture distributions.

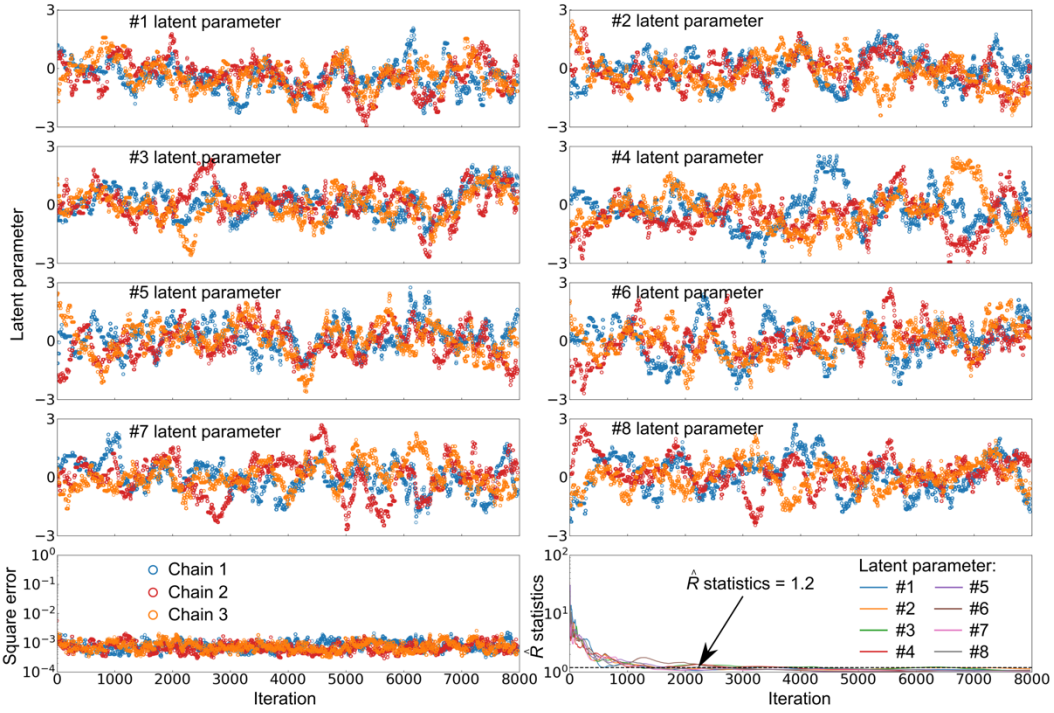


**Figure 5: Evolution of the first eight latent parameters (rows 1 to 4), square error between simulated and measured tracer data (left column in row 5), and $\hat{R}$ statistics for the eight latent parameters (right column in row 5, the black dash line denotes the $\hat{R}$ = 1.2 threshold).**

### 4.2 Posterior distributions of latent parameters

The posterior distributions of the first eight latent parameters are shown in Fig. 6. For some latent parameters such as the #6 and #8 latent parameters, the posterior distributions are similar to the prior distributions. While for the other latent parameters, the posterior distribution differs from the standard normal distribution, either with a non-zero value for the maximum probability density (latent parameters # 1, 4 and 7) or exhibits multimodal characteristics (latent parameters # 2, 3 and 5).

### 4.3 Aperture distribution and tracer breakthrough curves

With the 5000 posterior parameter samples from the 10 chains, we can analyze the aperture distribution in the hydraulic fracture. For each of the posterior latent parameter sets, we use equation (7) to generate the corresponding aperture distribution. The aperture distribution is then applied to the hydraulic fracture, and the tracer transport model is called to simulate tracer transport process in the hydraulic fracture and calculate tracer breakthrough curves at E1-PB and E1-OT. Fig. 7 shows four aperture distributions reconstructed from four randomly selected posterior latent parameter sets, and Fig. 8(a) further shows the mean and standard deviation of the aperture distribution reconstructed from all the 5000 posterior latent parameter sets. The aperture between the tracer injection point (E1-I) and the two tracer monitoring points (E1-PB and E1-OT) varies between 0.12 and 0.18 mm, and the standard deviation between the injection and monitoring

points is approximately 0.04 mm, indicating that the uncertainty of the aperture in this area is well constrained by the MCMC inference. However, the apertures out of this area cannot be constrained since their impact on the tracer breakthrough behavior at E1-PB and E1-OT is insignificant. Fig. 8(b) shows the 90% credible interval of the tracer breakthrough curves at E1-PB and E1-OT calculated from the 5000 posterior latent parameter sets. Both the two tracer breakthrough curves are appropriately reproduced with the posterior aperture distributions.

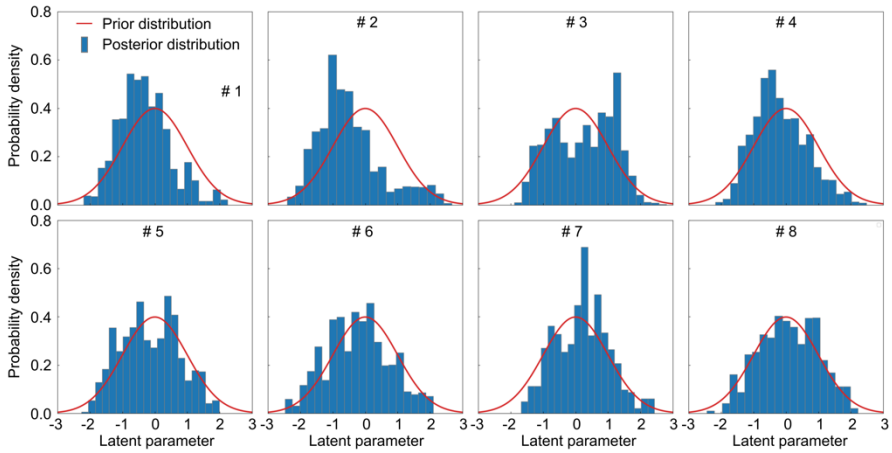


**Figure 6: Prior and posterior distributions of latent parameters. Only the first eight parameters are shown, as annotated by the number in each graph.**

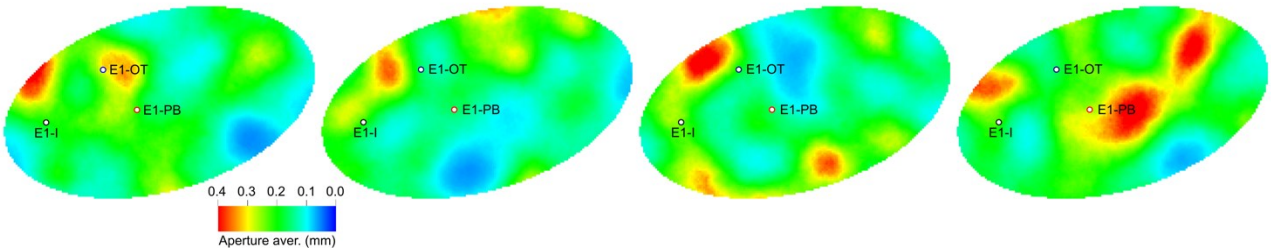


**Figure 7: Aperture distribution in the hydraulic fracture reconstructed from four posterior latent parameter sets.**

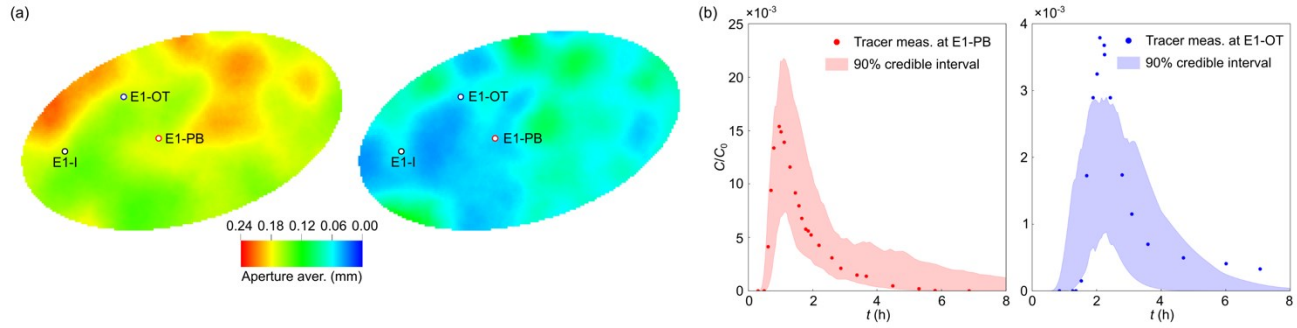


**Figure 8: Aperture distribution and tracer breakthrough curves inferred from MCMC. (a) Mean and standard deviation of the aperture distribution in the hydraulic fracture. (b) Comparison of tracer breakthrough curves between field measurements and modeling results.**

## 5. CONCLUDING REMARKS

In the present study, we use a deep learning accelerated MCMC framework to infer aperture distribution in a hydraulic fracture from tracer measurements. The dimensionality reduction of the original high-dimensional aperture distribution through PCA and the development of a surrogate model for tracer transport in the hydraulic fracture greatly improve the inference efficiency of MCMC. The posterior aperture distribution and the associated uncertainty are appropriately characterized. The results indicate that the aperture distribution between tracer injection and monitoring points can be well constrained through MCMC inference.

In the current study, we do not consider the approximation error caused by the replacement of tracer transport model with the surrogate model. There are two methods to address the approximation error in MCMC framework. The first method is the delayed acceptance MCMC in which the surrogate model is first used to evaluate the proposed sample, and if the sample is accepted, the tracer transport

model will be used to re-evaluate the sample and determine whether or not to accept the sample in the Markov chain (Efendiev et al., 2005; Laloy et al., 2013). The other method is to adaptively refine the surrogate model over the posterior distribution (Zhang et al., 2020b). Our future research will investigate the effectiveness of these methods to improve the accuracy of MCMC inference.

## ACKNOWLEDGEMENT

This material was based upon work supported by the U.S. Department of Energy, Office of Energy Efficiency and Renewable Energy (EERE), Office of Technology Development, Geothermal Technologies Office, under Award Number DE-AC52-07NA27344. Publication releases for this manuscript are under LLNL-CONF-819111. The United States Government retains, and the publisher, by accepting the article for publication, acknowledges that the United States Government retains a non-exclusive, paid-up, irrevocable, world-wide license to publish or reproduce the published form of this manuscript, or allow others to do so, for United States Government purposes. The research supporting this work took place in whole or in part at the Sanford Underground Research Facility in Lead, South Dakota. The assistance of the Sanford Underground Research Facility and its personnel in providing physical access and general logistical and technical support is acknowledged.

Support from the EGS Collab Team is gratefully acknowledged. EGS Collab Team includes J. Ajo-Franklin, T. Baumgartner, K. Beckers, D. Blankenship, A. Bonneville, L. Boyd, S. Brown, J.A. Burghardt, C. Chai, Y. Chen, B. Chi, K. Condon, P.J. Cook, D. Crandall, P.F. Dobson, T. Doe, C.A. Doughty, D. Elsworth, J. Feldman, Z. Feng, A. Foris, L.P. Frash, Z. Frone, P. Fu, K. Gao, A. Ghassemi, Y. Guglielmi, B. Haimson, A. Hawkins, J. Heise, C. Hopp, M. Horn, R.N. Horne, J. Horner, M. Hu, H. Huang, L. Huang, K.J. Im, M. Ingraham, E. Jafarov, R.S. Jayne, S.E. Johnson, T.C. Johnson, B. Johnston, K. Kim, D.K. King, T. Kneafsey, H. Knox, J. Knox, D. Kumar, M. Lee, K. Li, Z. Li, M. Maceira, P. Mackey, N. Makedonska, E. Mattson, M.W. McClure, J. McLennan, C. Medler, R.J. Mellors, E. Metcalfe, J. Moore, C.E. Morency, J.P. Morris, T. Myers, S. Nakagawa, G. Neupane, G. Newman, A. Nieto, C.M. Oldenburg, T. Paronish, R. Pawar, P. Petrov, B. Pietzyk, R. Podgorney, Y. Polsky, J. Pope, S. Porse, J.C. Primo, C. Reimers, B.Q. Roberts, M. Robertson, W. Roggenthen, J. Rutqvist, D. Rynders, M. Schoenball, P. Schwering, V. Sesetty, C.S. Sherman, A. Singh, M.M. Smith, H. Sone, E.L. Sonnenthal, F.A. Soom, P. Sprinkle, C.E. Strickland, J. Su, D. Templeton, J.N. Thomle, V.R. Tribaldos, C. Ulrich, N. Uzunlar, A. Vachaparampil, C.A. Valladao, W. Vandermeer, G. Vandine, D. Vardiman, V.R. Vermeul, J.L. Wagoner, H.F. Wang, J. Weers, N. Welch, J. White, M.D. White, P. Winterfeld, T. Wood, S. Workman, H. Wu, Y.S. Wu, E.C. Yildirim, Y. Zhang, Y.Q. Zhang, Q. Zhou, M.D. Zoback

## REFERENCES

Asher, M.J., Croke, B.F.W., Jakeman, A.J., Peeters, L.J.M.: A review of surrogate models and their application to groundwater modeling. *Water Resources Research*, **51**, (2015), 5957-5973.

Bianchi, L., Snow D.: Permeability crystalline rock interpretated from measured orientations and apertures of fractures. *Annu. Arid Zone*, **8**(2), (1968), 231-245.

Cacas, M.C., Ledoux, E., de Marsily, G., Barbreau, A., Calmels, P., Gaillard, B., et al.: Modeling fracture flow with a stochastic discrete fracture network: Calibration and validation. 2. The transport model. *Water Resources Research*, **26**(3), (1990), 491-500.

Canchumuni, S.W.A., Castro, J.D.B., Potratz, J., Emerick, A.A., Pacheco, M.A.C.: Recent developments combining ensemble smoother and deep generative networks for facies history matching. *Computational Geosciences*, **25**, (2021), 433-466.

Chen, X., Hammond, G.E., Murray, C.J., Rockhold, M.L., Vermeul, V.R., Zachara, J.M.: Application of ensemble-based data assimilation techniques for aquifer characterization using tracer data at Hanford 300 area. *Water Resources Research*, **49**, (2013), 7064-7076.

Christen, J.A., Fox, C.: Markov chain Monte Carlo using an approximation. *Journal of Computational and Graphical Statistics*, **14**, (2005), 795-810

Cui, T., Fox, C., O'Sullivan, M.J.: Bayesian calibration of a large-scale geothermal reservoir model by a new adaptive delayed acceptance Metropolis Hastings algorithm. *Water Resources Research*, **47**, (2011), W10521.

Efendiev, Y., Datta-Gupta, A., Ginting, V., Ma, X., Mallick, B.: An efficient two-stage Markov chain Monte Carlo method for dynamic data integration. *Water Resources Research*, **41**, (2005), W12423.

Falkner, S., Aaron, K., Frank, H.: BOHB: Robust and efficient hyperparameter optimization at scale. *International Conference on Machine Learning*, Stockholm, Sweden, 2018.

Fu, J., Gómez-Hernández, J.J.: Uncertainty assessment and data worth in groundwater flow and mass transport modeling using a blocking Markov chain Monte Carlo method. *Journal of Hydrology*, **364**, (2009), 328-341.

Fu, P., Settgast, R.R., Hao, Y., Morris, J.P., Ryerson, F.J.: The influence of hydraulic fracturing on carbon storage performance: hydraulic fracturing in carbon storage. *Journal of Geophysical Research: Solid Earth*, **122** (12), (2017), 9931-9949.

Gale, J. E.: Comparison of coupled fracture deformation and fluid flow models with direct measurements of fracture pore structure and stress-flow properties. 28th U.S. Symposium of Rock Mechanics, 1987.

Gelman, A., Rubin, D.B.: Inference from iterative simulation using multiple sequences. *Statistical Science*, **7**(4), (1992), 457-511.

Gierzynski, A.O., Pollyea, R.M.: Three-phase $CO_2$ flow in a basalt fracture network. *Water Resources Research*, **53**, (2017), 8980-8998.

Guo, B., Fu, P., Hao, Y., Peters, C.A., Carrigan, C.R.: Thermal drawdown-induced flow channeling in a single fracture in EGS. *Geothermics*, **61**, (2016), 46-62.

Haario, H., Saksman, E., Tamminen, J.: An adaptive Metropolis algorithm. *Bernoulli*, **7**, (2001), 223-242.

Hastings, W.K.: Monte Carlo sampling methods using Markov chains and their applications. *Biometrika*, **57**, (1970), 97-109.

Hawkins, A.J., Becker, M.W., Tester, J.W.: Inert and adsorptive tracer tests for Field measurement of flow-wetted surface area. *Water Resources Research*, **54**, (2018), 5341-5358.

Hawkins, A.J., Fox, D.B., Koch, D.L., Becker, M.W., Tester J.W.: Predictive inverse model for advective heat transfer in a planar fracture with heterogeneous permeability. *Water Resources Research*, **56**, (2020), e2020WR027065.

Kneafsey, T.J., Blankenship, D., Knox, H.A., Johnson, T.C., Ajo-Franklin, J.B., Schwering, P.C., et al.: EGS Collab project: Status and progress. 44th Stanford Geothermal Workshop, Stanford University, Stanford, CA, 2019.

Kneafsey, T.J., Blankenship, D., Dobson, P., Morris, J.P., White, M.D., Fu. P., et al.: The EGS Collab Project: Learning from Experiment 1. 45th Stanford Geothermal Workshop, Stanford University, Stanford, CA, 2020.

Laloy, E., Hérault, R., Lee, J., Jacques, D., Linde, N.: Inversion using a new low-dimensional representation of complex binary geological media based on a deep neural network. *Advances in Water Resources*, **110**, (2017), 387-405.

Laloy, E., Hérault, R., Jacques, D., Linde, N.: Training-image based geostatistical inversion using a spatial generative adversarial neural network. *Water Resources Research*, **54**, (2018), 381-406.

Laloy, E., Rogiers, B., Vrugt, J.A., Mallants, D., Jacques, D.: Efficient posterior exploration of a high-dimensional groundwater model from two-stage Markov Chain Monte Carlo simulation and polynomial chaos expansion. *Water Resources Research*, **49**, (2013), 2664-2682.

Laloy, E., Vrugt, J.A.: High-dimensional posterior exploration of hydrologic models using multiple-try DREAM (ZS) and high-performance computing. *Water Resources Research*, **48**, (2012), W01526.

Lu, H., Shen, Q., Chen, J., Wu, X., Fu, X.: Parallel multiple-chain DRAM MCMC for large-scale geosteering inversion and uncertainty quantification. *Journal of Petroleum Science and Engineering*, **174**, (2018), 189-200.

Marzouk, Y.M., Najm, H.N.: Dimensionality reduction and polynomial chaos acceleration of Bayesian inference in inverse problems. *Journal of Computational Physics*, **228**, (2009), 1862-1902.

Metropolis, N., Rosenbluth, A.W., Rosenbluth, M.N., Teller, A.H., Teller, E.: Equation of state calculations by fast computing machines. *The Journal of Chemical Physics*, **21**, (1953), 1087-1092.

Mo, S., Zabaras, N., Shi, X., Wu, J.: Integration of adversarial autoencoders with residual dense convolutional networks for estimation of non-Gaussian hydraulic conductivities. *Water Resources Research*, **56**, (2020), e2019WR026082.

Moreno, L., Tsang, Y.W., Tsang, C.F., Hale, F.V., Neretnieks, I.: Flow and tracer transport in a single fracture: A stochastic model and its relation to some field observations. *Water Resources Research*, **24**(12), (1988), 2033-2048.

Neuman, S.P.: Trends, prospects and challenges in quantifying flow and transport through fractured rocks. *Hydrogeology Journal*, **13** (1), (2015), 124-147.

Neupane, G., Mattson, E.D., Plummer, M.A., Podgorney, R.K., EGS Collab Team: Results of multiple tracer injections into fractures in the EGS Collab Testbed-1. 45th Stanford Geothermal Workshop, Stanford University, Stanford, CA, 2020.

Pyrak-Nolte, L.J., Morris, J.P.: Single fractures under normal stress: The relation between fracture specific stiffness and fluid flow. *International Journal of Rock Mechanics and Mining Sciences*, **37**, (2000), 245-262.

Radilla, G., Sausse, J., Sanjuan, B., Fourar, M.: Interpreting tracer tests in the enhanced geothermal system (EGS) of Soultz-sous-Forêts using the equivalent stratified medium approach. *Geothermics*, **44**, (2012), 43-51.

Razavi, S., Tolson, B.A., Burn, D.H.: Review of surrogate modeling in water resources. *Water Resources Research*, **48**, (2012), W07401.

Shakas, A., Linde, N., Le Borgne, T., Bour, O.: Probabilistic inference of fracture-scale flow paths and aperture distribution from hydrogeophysically-monitored tracer tests. *Journal of Hydrology*, **567**, (2018), 305-319.

Schoenball, M., Ajo-Franklin, J.B., Blankenship, D., Chai, C., Chakravarty, A., Dobson, P., et al.: Creation of a mixed-mode fracture network at mesoscale through hydraulic fracturing and shear Stimulation. *Journal of Geophysical Research: Solid Earth*, 125, (2020), e2020JB019807.

Somogyvári, M., Jalali, M., Jimenez Parras, S., Bayer, P.: Synthetic fracture network characterization with transdimensional inversion. *Water Resources Research*, **53**, (2017), 5104-5123.

Tang, M., Liu, Y., Durlofsky, L.J.: A deep-learning-based surrogate model for data assimilation in dynamic subsurface flow problems. *Journal of Computational Physics*, **413**, (2020), 109456.

ter Braak, C.J.F., Vrugt, J.A.: Differential Evolution Markov Chain with snooker updater and fewer chains. *Statistics and Computing*, **18**, (2008), 435-446.

Tsang, C.F., Neretnieks, I., Tsang, Y.: Hydrologic issues associated with nuclear waste repositories. *Water Resources Research*, **51**, (2015), 6923-6972.

Tsang, Y.W., Tsang, C.F.: Flow channeling in a single fracture as a two-dimensional strongly heterogeneous permeable medium. *Water Resources Research*, **25**(9), (1989), 2076-2080.

Vogt, C., Kosack, C., Marquart, G.: Stochastic inversion of the tracer experiment of the enhanced geothermal system demonstration reservoir in Soultz-sous-Forêts - Revealing pathways and estimating permeability distribution. *Geothermics*, **42**, (2012a), 1-12.

Vogt, C., Marquart, G., Kosack, C., Wolf, A., Clauser, C.: Estimating the permeability distribution and its uncertainty at the EGS demonstration reservoir Soultz-sous-Forêts using the ensemble Kalman filter. *Water Resources Research*, **48**, (2012b), W08517.

Vrugt, J.A.: Markov chain Monte Carlo simulation using the DREAM software package: Theory, concepts, and MATLAB implementation. *Environmental Modelling and Software*, **75**, (2016), 273-316.

White, M.D., Johnson, T.C., Fu, P., Wu, H., Ghassemi, A., Lu, J.R., et al.: The necessity for iteration in the application of numerical simulation to EGS: Examples from the EGS Collab test bed 1. 44th Stanford Geothermal Workshop, Stanford University, Stanford, CA, 2019.

Wu, H., Fu, P., Morris, J.P., Mattson, E.D., Neupane, G., Smith, M.M., et al.: Characterization of flow and transport in a fracture network at the EGS Collab field experiment through stochastic modeling of tracer recovery. *Journal of Hydrology*, **593**, (2021), 125888.

Wu, H., Fu, P., Zhang, J., Morris, J.P.: Interpretation of tracer data using a Markov chain Monte Carlo approach for the characterization of the EGS Collab testbed, 54th US Rock Mechanics/Geomechanics Symposium, Golden, Colorado, USA, 2020.

Zagoruyko, S., Komodakis, N.: Wide residual networks. British Machine Vision Conference, British Machine Vision Association, 2016.

Zhang, D., Lu, Z.: An efficient, high-order perturbation approach for flow in random porous media via Karhunen-Loève and polynomial expansions. *Journal of Computational Physics*, **194**, (2004), 773-794.

Zhang, J., Man, J., Lin, G., Wu, L., Zeng, L.: Inverse modeling of hydrologic systems with adaptive multifidelity Markov Chain Monte Carlo simulations. *Water Resources Research*, **54**, (2018), 4867-4886.

Zhang, J., Taflanidis, A.A.: Accelerating MCMC via Kriging-based adaptive independent proposals and delayed rejection. *Computer Methods in Applied Mechanics and Engineering*, **355**, (2019), 1124-1147.

Zhang, J., Vrugt, J.A., Shi, X., Lin, G., Wu, L., Zeng, L.: Improving simulation efficiency of MCMC for inverse modeling of hydrologic systems with a Kalman-inspired proposal distribution. *Water Resources Research*, **56**, (2020a), e2019WR025474.

Zhang, J., Zheng, Q., Chen, D., Wu, L., Zeng, L.: Surrogate-based Bayesian inverse modeling of the hydrological system: An adaptive approach considering surrogate approximation error. *Water Resources Research*, **56**, (2020b), e2019WR025721.

Zhong, Z., Sun, A.Y., Jeong, H.: Predicting $CO_2$ plume migration in heterogeneous formations using conditional deep convolutional generative adversarial network. *Water Resources Research*, **55**, (2019), 5830-5851.